How to cite: *Angew. Chem. Int. Ed.* **2021**, *60*, 19222–19231
International Edition: doi.org/10.1002/anie.202104709
German Edition: doi.org/10.1002/ange.202104709

Polyelectrolytes Hot Paper

Heteroaromatic Hyperbranched Polyelectrolytes: Multicomponent Polyannulation and Photodynamic Biopatterning

Xiaolin Liu[+], Minghui Xiao[+], Ke Xue, Mingzhao Li, Dongming Liu, Yong Wang, Xinzhe Yang, Yubing Hu, Ryan T. K. Kwok, Anjun Qin, Chunlei Zhu, Jacky W. Y. Lam,* and Ben Zhong Tang**

Dedicated to the 30th anniversary of The Hong Kong University of Science and Technology and the 100th anniversary of Chemistry at Nankai University

Abstract: *We reported an efficient multicomponent polyannulation for in situ generation of heteroaromatic hyperbranched polyelectrolytes by using readily accessible internal diynes and low-cost, commercially available arylnitriles, $NaSbF_6$, and H_2O/AcOH. The polymers were obtained in excellent yields (up to 99%) with extraordinary high molecular weights (M_w up to 1.011×10^6) and low polydispersity indices. The resulting polymers showed good processibility and high quantum yields with tunable emission in the solid state, making them ideal materials for highly ordered fluorescent photopatterning. These hyperbranched polyelectrolytes also possessed strong ability to generate reactive oxygen species, which allowed their applications in efficient bacterial killing and customizable photodynamic patterning of living organisms in a simple and cost-effective way.*

Introduction

Polyelectrolytes, such as DNA, RNA, and proteins, are widespread in natural living systems, and possess biological properties and multiple charges to interact with oppositely charged species via electrostatic attraction.[1] Among various natural polyelectrolytes, polysaccharides are the largest component of biomass, exemplified by a variety of hyperbranched species,[2] such as amylopectin,[3] glycogen,[4] arabinoxylan,[5] xanthan gum,[6] and PTR-EPS1.[7] In general, these hyperbranched polysaccharides are rich in hydroxyl groups, while some of them contain additional amino groups, carboxyl groups, and sulfonate groups, which can be ionized under certain conditions to become hyperbranched polyelectrolytes to fulfill certain biological functions. Despite hyperbranched polyelectrolytes play a pivotal role in organisms, their exact chemical structures are hardly identified due to the structural complexity.[2] In addition, the contents of some species are low in nature.[7] Thus, understanding their detailed formation mechanisms and biological functions becomes difficult. In this regard, synthetic polymers can serve as largely accessible substitutes to mimic the structures and functions of biomacromolecules.[8] It is thus of great importance to design and synthesize novel hyperbranched polyelectrolytes and explore their potential applications.

Owing to the limited synthetic approach, the research progress of hyperbranched polyelectrolytes is stagnant. Typically, hyperbranched polymers are synthesized via the polycondensation of AB_2 monomers,[9] which lack chemical stability, require nontrivial synthetic efforts, and suffer from unsatisfactory functionality.[10] Another most widely used method is the copolymerization of A_3 and B_2 monomers,[11]

[*] Dr. X. Liu,[+] Dr. Y. Wang, Dr. Y. Hu, Dr. R. T. K. Kwok, Dr. J. W. Y. Lam, Prof. B. Z. Tang
Department of Chemistry, Hong Kong Branch of Chinese National Engineering Research Center for Tissue Restoration and Reconstruction, Institute for Advanced Study, Division of Biomedical Engineering, Division of Life Science, and State Key Laboratory of Molecular Neuroscience
The Hong Kong University of Science and Technology
Clear Water Bay, Kowloon, Hong Kong (China)
E-mail: chjacky@ust.hk
tangbenz@ust.hk

M. Xiao,[+] K. Xue, Prof. C. Zhu
Key Laboratory of Functional Polymer Materials of Ministry of Education, State Key Laboratory of Medicinal Chemical Biology, Institute of Polymer Chemistry, College of Chemistry
Nankai University, Tianjin 300071 (China)
E-mail: chunlei.zhu@nankai.edu.cn

Dr. X. Liu,[+] Dr. J. W. Y. Lam, Prof. B. Z. Tang
HKUST-Shenzhen Research Institute
No. 9 Yuexing 1st RD, South Area, Hi-tech Park, Nanshan
Shenzhen 518057 (China)

M. Li, D. Liu, X. Yang, Prof. A. Qin, Prof. B. Z. Tang
Center for Aggregation-Induced Emission, SCUT-HKUST Joint Research Institute, State Key Laboratory of Luminescent Materials and Devices, South China University of Technology
Guangzhou 510640 (China)

Prof. B. Z. Tang
AIE Institute
Guangzhou Development District, Huangpu
Guangzhou 510530 (China)
and
Guangdong-Hong Kong-Macau Joint Laboratory of Optoelectronic and Magnetic Functional Materials (China)
and
Shenzhen Institute of Molecular Aggregate Science and Engineering, School of Science and Engineering
The Chinese University of Hong Kong
Shenzhen, 2001 Longxiang Boulevard, Longgang District
Shenzhen City, Guangdong 518172 (China)

[+] These authors contributed equally to this work.

Supporting information and the ORCID identification number(s) for the author(s) of this article can be found under: https://doi.org/10.1002/anie.202104709.

which generally requires strictly controlled conditions to avoid gelation, large dispersity ($Đ$), and/or the formation of oligomeric products.[12] On the other hand, the main strategy for the synthesis of polyelectrolytes is the post-modification of nonionic polymers,[13] which is hard to achieve 100% conversion efficiency and leaves patches along the polymer chains. Some coupling reactions (e.g., Heck and Sonogashira) are also employed for the synthesis of polyelectrolytes, but they typically require expensive ionic monomers.[14] Besides, the aforementioned polymerizations are one or two-component systems, which greatly restrict the structural and functional diversity of polymers. In contrast with these "few-body" systems, the "many-body" systems are commonly adopted by natural polymerizations because the permutations and combinations of multiple components can bring in rich biodiversity and infinite possibilities.[15] As such, it is essential to develop multicomponent polymerizations for the facile synthesis of hyperbranched polyelectrolytes from stable monomers.

The development of novel hyperbranched polyelectrolytes with unique structures and multifunctionalities is still in strong demand. Although many hyperbranched polyelectrolytes have been studied during the past several decades,[16] most of them are commodity polymers with aliphatic backbones and no advanced functionalities.[17] In addition, the investigation of aromatic hyperbranched polymers often suffers from low molecular weight, poor processability, and poor solubility due to π–π stacking, which discourage their real-world applications. In this regard, the introduction of positively charged heteroaromatic fused rings into the hyperbranched polymers can probably address these issues and provide more opportunities. On the one hand, the heteroaromatic fused rings can endow the polymers with unique photophysical properties. Since the positively charged heteroaromatic rings are highly electron-deficient, they can act as appropriate donors to facilitate the formation of donor-acceptor (D-A) structures to tune the emission wavelength of polymers. On the other hand, the charges on the aromatic rings also help suppress intermolecular and/or intramolecular π–π stacking[18] to increase the solubility and processibility of polymers.

The heteroaromatic hyperbranched polyelectrolytes with unique physiochemical properties are expected to open new frontiers in their applications. On the one hand, the compact hyperbranched structure helps rigidify the luminescent units, which impedes the nonradiative decay by restricting intramolecular motions to result in fluorescent emission and intersystem crossing (ISC).[19] Such polymers are anticipated to show high fluorescence quantum yields desired for fluorescence imaging.[20] On the other hand, the polymers may undergo efficient ISC to a long-lived T_1 state and interact with adjacent triplet oxygen to produce reactive oxygen species (ROS) for photodynamic therapy (PDT).[21] Further, given the high charge density in the backbone, these polymers may exhibit affinity to negatively charged species in biological systems, such as DNA and bacterial membrane.[14,22] Besides, due to the eco-friendly and non-invasive attributes as well as the high spatiotemporal resolution of light,[23] PDT is promising for the precise patterning of living organisms, which offer an opportunity to build various kinds of bio-architectures in a cost-efficient way.

Herein, we developed a four-component ($AB_2 + C_2 + D + E$), seven-functional group polymerization approach, in which low-cost, commercially available arylnitriles and readily accessible internal diynes were reacted via rhodium(III)-catalyzed three-fold C–H activation in the presence of $NaSbF_6$ and H_2O/acetic acid (AcOH) to in situ generate heteroaromatic hyperbranched polyelectrolytes (Scheme 1).[24] These polymers were generated in excellent yields (up to 99%) with extraordinary high molecular weights (M_w up to 1.011×10^6) and low $Đ$ values. Surprisingly, these hyperbranched polyelectrolytes were luminescent in the solid state with tunable emission wavelength, high quantum yield, and good processibility, which made them ideal materials for fluorescent photopatterning. Because of their net positive charges and strong ROS generation ability, these polymers could serve as effective photosensitizers for photodynamic killing of bacteria. More interestingly, we, for the first time,

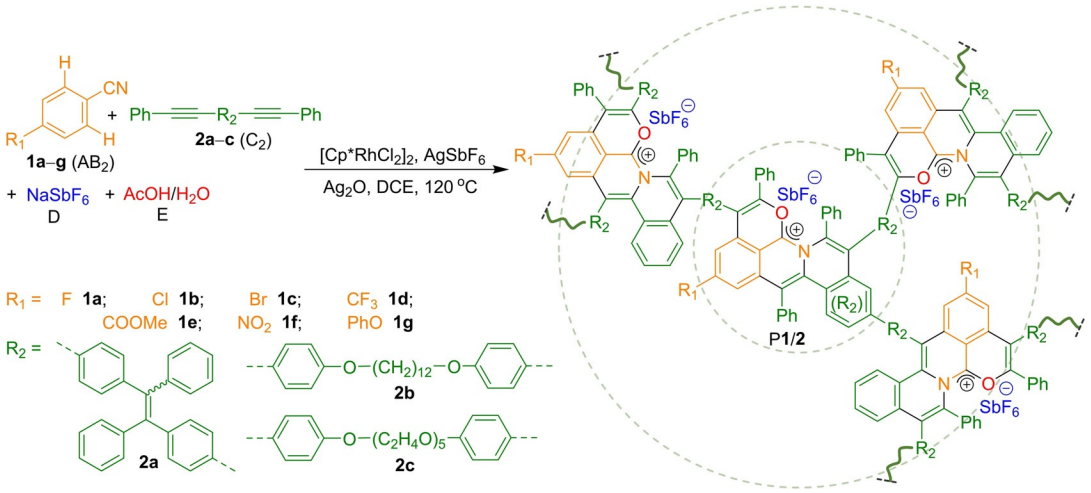

Scheme 1. In situ generation of heteroaromatic hyperbranched polyelectrolytes by polyannulation of arylnitriles, internal diynes, $NaSbF_6$, and $AcOH/H_2O$.

achieved the photodynamic patterning of living organisms in a customizable fashion and investigated the dynamic changes of the resulting biopatterns.

Results and Discussion

All monomers used in this work were easily acquired and chemically stable under ambient conditions. Arylnitriles **1a**–**g**, sodium hexafluoroantimonate(V) ($NaSbF_6$), and AcOH were low-cost and commercially available, and were directly used without further purification. The internal diynes **2a**–**c** involved in this work were facilely synthesized in high yields according to the previously reported procedures (Supporting Information, Scheme S1).[25] All polymerizations were catalyzed by $[Cp^*RhCl_2]_2$, Ag_2O, and $AgSbF_6$ in a one-pot manner.

To obtain soluble hyperbranched polyelectrolytes in high yields and high molecular weights, we systematically investigated the polymerization conditions using **1a**, **2a**, $NaSbF_6$, and AcOH/H_2O as monomers. Several key reaction parameters were set as variables to examine their impacts on the resulting polymers, including solvent type, monomer concentration, monomer ratio, catalyst loading, reaction atmosphere, and reaction time (Table 1). The effect of solvents on the polymerization was first studied (Table 1, entries 1–3). By comparing the polymerization reactions in 1,2-dichloroethane (DCE), dimethylsulfoxide (DMSO), and dichloromethane/methanol (DCM/MeOH, v/v, 1/1), the best result was obtained in pure DCE, which gave a polymer with a weight-average molecular weight (M_w) of 260 600 in 57% yield (entry 1). Increasing the concentration of **2a** from 50 to 100 mM led to a sharp decrease in both M_w and yield due to the incomplete dissolution of **2a** (entry 4). However, when the concentration of **2a** was decreased from 50 to 30 mM, the polymerization proceeded smoothly without gel formation even when the reaction time was extended from 12 to 18 h, affording a polymer with M_w of 231 400 in 84% yield (entry 5). It was found that the monomer ratio and catalyst loading also played crucial roles in the polymerization (entries 5–9). When the theoretical monomer loading ratio of [**1a**]:[**2a**] = 3:2 was adopted, a polymer with a high M_w was obtained in a high yield (entry 5). However, further increasing the amount of arylnitrile **1a** or internal diyne **2a** led to a sharp decrease in yield (entries 6–7). On the other hand, decreasing the loading of $[Cp^*RhCl_2]_2$ from 10 to 5% mol afforded a polymer with a higher M_w in a higher yield (entry 8). However, both M_w and yield were sharply decreased by further reducing the amount of $[Cp^*RhCl_2]_2$ (entry 9). The polymerization could also proceed in air without inert gas protection, affording a polymer with M_w of 29 700 in 61% yield (entry 10). A time of 18 h was eventually adopted as the optimal reaction time, as prolonging the reaction time to 24 h did not give rise to much higher M_w and yield (entry 11).

Under the optimized polymerization conditions, different arylnitriles and internal diynes were combined to evaluate the robustness and universality of this polymerization (Table 2), in which arylnitriles **1a**–**g** possessed substituent groups with different electron densities and steric hindrance, and internal diynes **2a**–**c** carried rigid conjugated or flexible spacers. As shown in Table 2, arylnitriles **1a**–**g** all reacted efficiently with internal diynes **2a**–**c** to give hyperbranched polyelectrolytes in excellent yields with high molecular weights (M_w up to 1.011×10^6). It is noteworthy that, the molecular weight of a hyperbranched polymer is often underestimated when measured by GPC using linear polystyrene as a standard, which is attributed to the contracted conformation and the reduced free volume of the globular hyperbranched polymer.[26] Indeed, when the molecular weight of the hyperbranched polyelectrolytes were measured by a multiangle laser light-scattering method, their absolute M_w values were 9–38 times of the polystyrene-calibrated ones (Table 2, entries 6–9). Sur-

Table 1: Optimization of the polyannulation reaction.[a]

Entry	Solvent	[**1a**] [mM]	[**2a**] [mM]	[Rh] [%]	time [h]	yield [%]	M_w[b]	$Đ$[b]
1	DCE	33	50	10	12	57	260 600	2.1
2	DCM/MeOH	33	50	10	12	trace		
3	DMSO	33	50	10	12	trace		
4	DCE	67	100	10	12	trace		
5	DCE	20	30	10	18	84	231 400	1.9
6	DCE	20	40	10	18	24	208 300	6.7
7	DCE	25	30	10	18	trace		
8	**DCE**	**20**	**30**	**5**	**18**	**97**	**307 100**	**2.1**
9	DCE	20	30	2.5	18	65	46 400	1.7
10[c]	DCE	20	30	5	18	61	29 700	1.3
11	DCE	20	30	5	24	99	417 800	1.6

[a] Unless otherwise noted, the polymerizations were carried out at 120 °C in N_2, with the addition of $NaSbF_6$ (4 equiv), H_2O (12 equiv), AcOH (9 equiv), $AgSbF_6$ (20 mol%), and Ag_2O (6 equiv).
[b] Estimated by GPC in DMF on the basis of a linear polystyrene calibration. $Đ$ = dispersity = M_w/M_n.
[c] The reaction was conducted in air.

Table 2: Polyannulation results with different monomers.[a]

Entry	Monomer	Yield [%]	M_w[b] (MALLS)[c]	$Đ$[b]
1	**1a/2a**	97	307 100	2.1
2	**1c/2a**	87	198 800	2.3
3	**1d/2a**	96	124 000	2.2
4	**1e/2a**	94	482 200	1.6
5	**1a/2b**	83	35 300	1.5
6	**1b/2c**	84	35 400 (328 200)	1.5
7	**1e/2c**	91	51 300 (719 800)	1.7
8	**1f/2c**	93	25 800 (652 800)	1.3
9	**1g/2c**	76	26 000 (1 011 000)	1.3

[a] Unless otherwise noted, the polymerizations were carried out at 120 °C in DCE under N_2 for 18 h, with [**1**] = 20 mM, [**2**] = 30 mM, $NaSbF_6$ (4 equiv), H_2O (12 equiv), AcOH (9 equiv), $AgSbF_6$ (20 mol%), $[Cp^*RhCl_2]_2$ (5 mol%), and Ag_2O (6 equiv). [b] Estimated by GPC in DMF on the basis of a linear polystyrene calibration. $Đ$ = dispersity = M_w/M_n. [c] Value measured by multiangle laser light scattering (MALLS) technique in THF.

prisingly, although hyperbranched materials synthesized by conventional polymerization approaches typically exhibited very broad $Đ$ (often exceeding 5–10),[27] the $Đ$ values of the present polymers were all lower than 2.3. The low $Đ$ values were probably caused by the large steric fused rings, which significantly suppressed the random cross-linking and gelation during the polymerization.

Based on the mechanism of a previously reported organic reaction,[24] we proposed a reaction mechanism for this multicomponent polyannulation (Scheme S3). Thanks to the C–H activation, two C–H bonds of the arylnitriles served as the hidden functional groups to participate in the polymerization process, and the three-fold C–H activation/annulation cascade of monomers allowed the polyelectrolytes to grow in three directions, resulting in hyperbranched polyelectrolytes with eight possible isomers in the chemical structures (Figure S1).

All the obtained heteroaromatic hyperbranched polyelectrolytes showed good solubility in commonly used organic solvents, such as DCM, chloroform, DCE, acetone, DMSO, and *N*,*N*-dimethylformamide (DMF), regardless of their molecular weights and the size of the fused-ring moieties. The thermal property of these polymers was evaluated by thermogravimetric analysis. The decomposition temperature at 5% weight loss under nitrogen was in the range of 201–257 °C (Figure S2), suggesting the high thermal stability of the present polymers. It is noteworthy that **P1d/2a** retained more than 60% of its initial weight even after heated to 800 °C, enabling it an ideal ceramic material.

To facilitate the structural characterization of the hyperbranched polyelectrolytes, model compound **3** was prepared by rhodium(III)-catalyzed cascade annulation of 4-fluorobenzonitrile and diphenylacetylene under the same synthetic conditions for the polymers (Scheme S2), and its spectral properties were in good accordance with the literature.[24] Typical FTIR, ^{1}H NMR, ^{13}C NMR, and ^{19}F NMR spectra of model compound **3**, polymer **P1a/2b**, and its corresponding monomers **1a** and **2b** were collected for comparative illustration. In the FTIR spectra (Figure 1), the C≡N stretching vibrations of **1a** and the C≡C stretching vibrations of **2b** occurred at 2233 and 2220 cm^{-1}, respectively. However, these peaks were not observed in the spectra of **3** and **P1a/2b**. Meanwhile, new peaks associated with the delocalized C=O, C=N, and Sb-F stretching vibrations emerged in the spectra of **P1a/2b** at 1741, 1641, and 657 cm^{-1}, respectively, indicating the occurrence of the polymerization. Similar observations were also found in the FTIR spectra of other polymers (Figure S3 and S4).

The ^{1}H NMR and ^{13}C NMR spectra of monomers **1a** and **2b**, model compound **3** and **P1a/2b** in CD_2Cl_2 were compared and shown in Figure S6. New peaks emerged at $\delta = 7.76$ in the spectra of **3** and **P1a/2b**, corresponding to the aromatic proton absorptions from the newly formed heteroaromatic fused rings (Figure S6C,D). Besides, the ^{13}C NMR spectra further verified our hypothesis on the chemical structure of the resulting polymer (Figure S6E–H). The characteristic peak of C≡N in **1a** was not observed in the polymer spectrum, and, meanwhile, the intensity of the characteristic C≡C peak in **2b** was sharply decreased in the polymer spectrum as

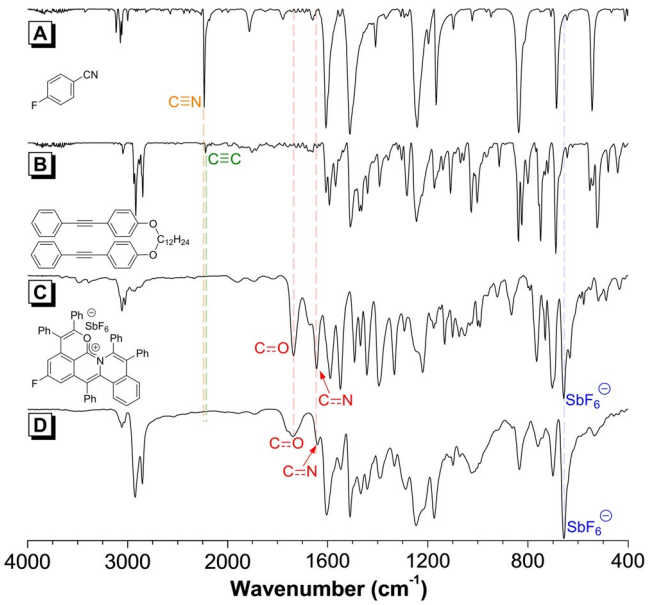

Figure 1. FTIR spectra of A) **1a**, B) **2b**, C) Model **3**, and D) **P1a/2b**.

a result of polyannulation. Instead, the aromatic carbons at positions "d" resonated at $\delta = 170.69$ and 170.71 in the spectra of **3** and **P1a/2b**, respectively. Similar features were also observed in the spectra of other polymers (Figure S7–S31), confirming the successful synthesis of polymers with structures as shown in Scheme 1. However, the degree of branching of the hyperbranched polyelectrolytes was difficult to be derived from ^{1}H, ^{13}C or ^{19}F NMR spectra because of the overlapping of the resonances and broad signals arising from structural isomerism.

Motivated by the unique heteroaromatic fused-ring moieties in the molecular structures, we systematically studied the photophysical properties of the model compound and polymers. The absorption spectra of the model compound and polymers in chloroform (10 μM) were shown in Figure S32. Their maximum absorption peaks were found in the range of 480–548 nm. By incorporating different substituent groups to the strong electron-withdrawing heteroaromatic fused rings, the maximum emission wavelength of the polymers could be facilely tuned from 575 to 652 nm (Figure 2A). In particular, by introducing tetraphenylethylene (TPE) into the polymer skeletons, the resulting polymers **P1a/2a** and **P1c–e/2a** showed aggregation-enhanced emission. Taking **P1e/2a** as an example, its chloroform solution fluoresced weakly at 619 nm. Upon the addition of hexane, a nonpolar poor solvent for the polymer, into the chloroform solution, the emission intensity gradually increased accompanied with a slight blueshift in the emission maximum to 612 nm (Figure 2B and Figure S33). We further examined the solid fluorescence of the as-synthesized model compound and polymers. The emission of **3** and **P1/2** powders covered the spectral range from yellow, orange, and red to deep red with a gradual shift in maximum emission wavelength from 570 to finally 662 nm (Figure 2C and Figure S34). In general, the synthesis of conventional red/deep red luminogens require tedious synthetic steps because of the inclusion of π-

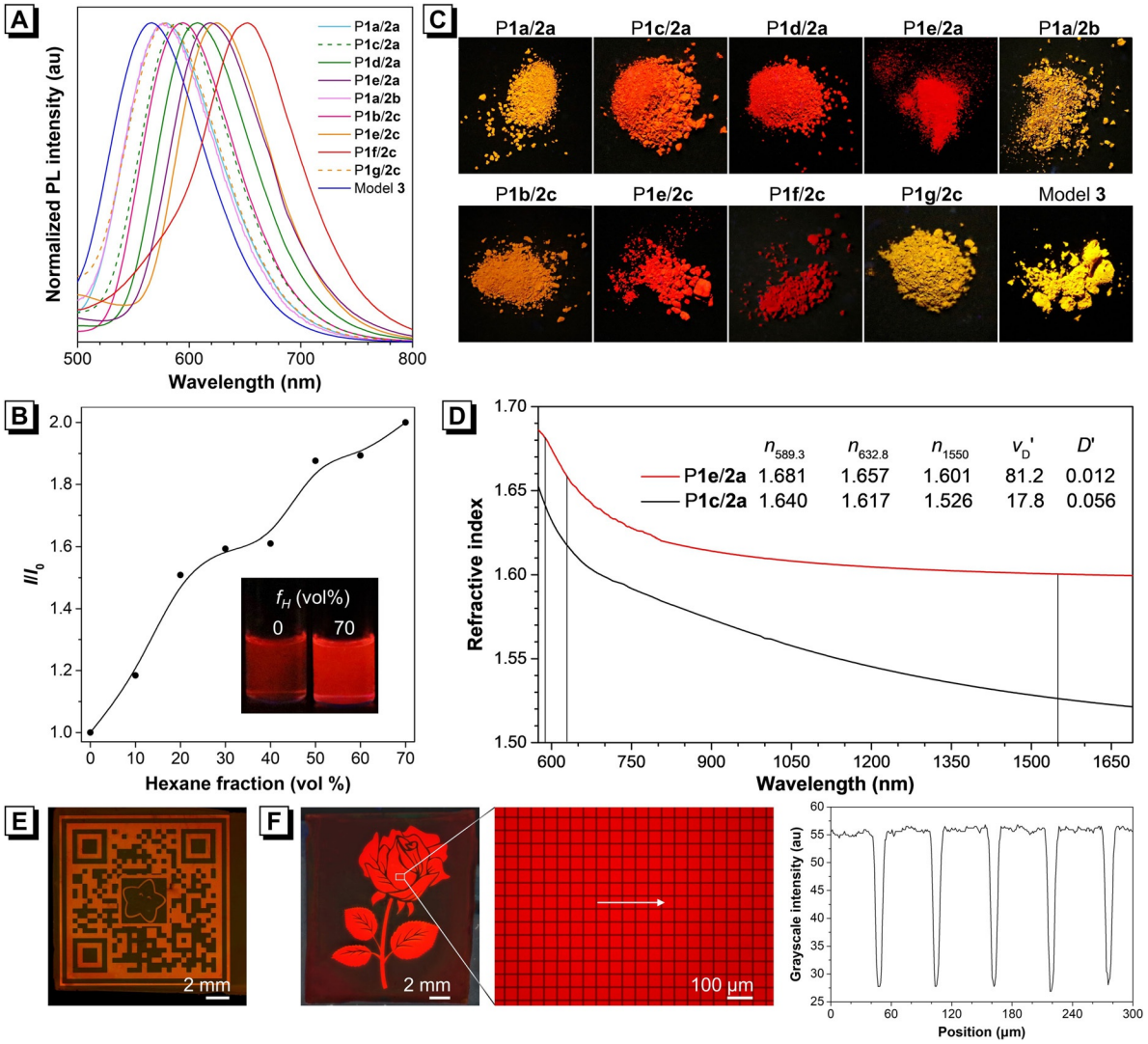

Figure 2. Photophysical and optical properties of model **3** and P**1**/**2**. A) Emission spectra of P**1**/**2** and model **3** in chloroform. Concentration: 10 μM. Excitation wavelength: 365 nm. B) Plot of relative emission intensity (I/I_0) versus the composition of hexane/chloroform mixtures of P**1e**/**2a**. Inset: Photographs of P**1e**/**2a** in hexane/chloroform mixtures with different hexane fractions (f_H) taken under UV irradiation from a handheld UV lamp. Concentration: 1 μM. I_0 = PL intensity in pure chloroform. Excitation wavelength: 365 nm. C) Luminescent photographs of polymer P**1**/**2** and model **3** in the solid state. D) Wavelength dependence of refractive index of thin films of P**1c**/**2a** and P**1e**/**2a**. Abbreviation: n = refractive index, ν_D' = modified Abbé number = $(n_{1319}-1)/(n_{1064}-n_{1559})$, D' = chromatic dispersion = $1/\nu_D'$. E) Two-dimensional fluorescent photopatterns generated by photolithography of films of P**1c**/**2a**. (F) Two-dimensional fluorescent photopatterns generated by photolithography of films of P**1e**/**2a** with zoom-in form (left) and the grayscale intensity profile of the arrowed area (right).

conjugated macrocyclic units. In addition, the resulting polymers often suffer from aggregation-caused quenching to result in a low quantum yield in the solid state.[28] Notably, the thin films of P**1**/**2** showed high photoluminescence quantum yields (PLQY) of up to 14.3% (Table S1). Particularly, the red-emissive P**1e**/**2a** film exhibited a PLQY of 6.7% with CIE coordinates of (0.63, 0.36) (Figure S35). The photostability study showed that the P**1e**/**2a** film retained more than 70% of its initial absorbance when irradiated by white light at a power density of 100 mW cm^{-2} for 60 min, indicating its good photostability (Figure S36). The efficient solid-state emission of the polymers indicated their great potential as light-emitting coating materials and fluorescent sensors.

High-refractive-index polymers are promising candidate materials for optical engineering applications, such as optical chips, prisms, optical waveguides, and holographic image recording systems.[29] Polarizable aromatic rings and heteroatoms (particularly halogen elements) are well-known contributors for enhancing the refractive index (n).[30] In view of the unique chemical structure, we measured the n values of the synthesized polymers with polarized heteroaromatic fused rings by using P**1c**/**2a** and P**1e**/**2a** for demonstration. As summarized in Figure 2D, both polymers showed high n values with small chromic dispersion. Interestingly, P**1e**/**2a** possessed high n values of 1.686–1.600 in the spectral region of 575–1690 nm, which were higher than those of some inorganic gems, such as emerald ($n_{1079.5}$ = 1.566 and $n_{1341.4}$ =

1.560), and much higher than those of the commercial optical polymers, such as polycarbonate ($n_{632.8}=1.581$), poly(methyl methacrylate) ($n_{632.8}=1.489$ and $n_{1550}=1.481$), and polydimethylsiloxane ($n_{632.8}=1.428$).[31]

The generation of highly ordered macro- and microfluorescent patterns by photolithography is of great significance for the construction of optical display devices, optical writing and reading, and anti-counterfeiting applications.[32] Thanks to the excellent film-forming ability and efficient solid-state emission of the present polymers, it is possible to fabricate their uniform fluorescent films without defects on silica wafers by a simple spin-coating technique. Upon exposing the polymer thin films to UV light at room temperature for 40 min under a customizable photomask, the fluorescence of the exposed regions was completely quenched due to the photo-oxidation of the chromophores,[25] whereas the masked regions remained intact and highly emissive (Figure 2E), which favored the generation of a fluorescent QR code pattern. In addition to macro-pattern, other sophisticated patterns with varying sizes and contents could also be readily generated by changing the scale and shape of the photomask. As shown in Figure 2F, a fluorescent rose-shaped macro-pattern was easily created. When examining the enlarged image of a selected location, it was found that each region in the macro-pattern was actually composed of gridlike micro-pattern with sharp edges, indicating the high resolution and structural complexity. The facile, rapid, and precise generation of highly emissive patterns demonstrated the promise of the present polymers in photonic and electronic applications.

Heteroaromatic cations such as pyridinium salts and quinolizinium salts have been reported to be typical acceptor groups for efficient generation of ROS.[19b,33] In this regard, the novel heteroaromatic, carbocationic moieties in the present polyelectrolytes encouraged us to explore their ROS generation ability. Two commercial ROS indicators, including 2′,7′-dichlorofluorescin (DCFH) and 9,10-anthracenediyl-bis(methylene)dimalonic acid (ABDA), were used to evaluate ROS generation of the P**1c**/**2a**, P**1d**/**2a**, P**1e**/**2a**, and P**1e**/**2c** as demonstration. DCFH is a nonfluorescent probe, but can be converted to the highly fluorescent form (2′,7′-dichlorofluorescein; DCF) when oxidized by various ROS. As shown in Figure 3A and Figure S37, in the absence of polymers, DCFH remained nonfluorescent even upon white-light irradiation (8 mW cm^{-2}). In contrast, in the presence of polymers and white-light irradiation, the emission associated with DCF at 524 nm was significantly increased, indicating that these polymers could be used to sensitize the generation of ROS.

Singlet oxygen ($^1O_2$) is one of the important ROS species with significant applications in several fields, including organic synthesis and photodynamic therapy.[34] It is thus essential to measure the $^1O_2$ generation ability of these polymers. In the presence of $^1O_2$, the absorption of ABDA became weakly due to its conversion to endoperoxide. Thus, under white-light irradiation, we recorded the absorbance spectra of ABDA in the presence of P**1e**/**2a**, P**1c**/**2a**, P**1d**/**2a**, and P**1e**/**2c** (Figure 3B and Figure S38). For comparison, the performance of Rose Bengal, a most widely used photosensitizer for $^1O_2$ generation, was also tested under the same condition. In the presence of polyelectrolytes and white-light irradiation, a noticeable decrease of ABDA absorption at 378 nm was observed. Specifically, the $^1O_2$ generation efficiency of P**1e**/**2a** was much higher than Rose Bengal. P**1c**/**2a** and P**1d**/**2a** were also able to generate $^1O_2$ more effectively than Rose Bengal, but P**1e**/**2c** showed inferior performance. According to a method reported in previous studies,[35] the $^1O_2$ quantum yields of P**1c**/**2a**, P**1d**/**2a**, P**1e**/**2a**, and P**1e**/**2c** were determined to be 0.943, 0.899, 0.975, and 0.375, respectively (Figure S39). The strong $^1O_2$ generation efficiency of P**1c**–**e**/**2a** was probably ascribed to its conjugated D-A structure, which significantly reduced the singlet-triplet energy gap and promoted the intersystem crossing (ISC) process. On the other hand, the compact hyperbranched structures of P**1c**–**e**/**2a** rigidified the intramolecular motions of the polymer backbones, which suppressed the nonradiative decay and facilitated the ISC process. Although P**1e**/**2c** also possessed a strong D-A pair in the polymer structure, its $^1O_2$ generation ability was quite low due to the active intramolecular motions induced by the flexible oligo(ethylene glycol) chains, which consumed the excited-state energy nonradiatively.

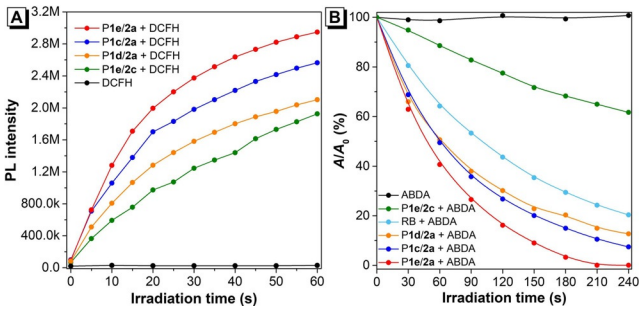

Figure 3. Reactive oxygen species (ROS) generation of P**1**/**2**. A) Changes of fluorescence intensity at 524 nm of 2′,7′-dichlorofluorescin (DCFH) in the presence or absence of P**1c**/**2a**, P**1d**/**2a**, P**1e**/**2a**, and P**1e**/**2c** in aqueous suspension with white-light irradiation for different time periods. B) The decomposition rates of 9,10-anthracenediyl-bis(methylene)dimalonic acid (ABDA) by P**1c**/**2a**, P**1d**/**2a**, P**1e**/**2a**, P**1e**/**2c**, and Rose Bengal (RB), where A_0 and A are the absorbance of ABDA in the presence of photosensitizers at 378 nm before and after white-light irradiation, respectively.

The strong $^1O_2$ generation ability of the polymers encouraged us to further explore their potential in photodynamic killing of bacteria. P**1e**/**2a**, the strongest photosensitizer for ROS generation, was chosen for subsequent biological experiments. We first characterized the particle size and zeta potential of P**1e**/**2a** aggregates upon addition of its solution to phosphate buffered saline (PBS). The hydrodynamic diameter of P**1e**/**2a** aggregates ranged from 70–150 nm with a zeta potential of 7.79 ± 0.75 mV (Figure 4A). Furthermore, we also performed transmission electron microscopy (TEM) characterization to confirm the particle size (Figure 4A inset). Because of its positive charge, P**1e**/**2a** tended to accumulate on the negatively charged bacterial membrane through electrostatic interactions. Such property enabled fluorescent labeling of methicillin-resistant *Staphylococcus aureus* (MRSA) by P**1e**/**2a** within 60 min (Figure 4B). Next, we evaluated the quantitative inactivation of

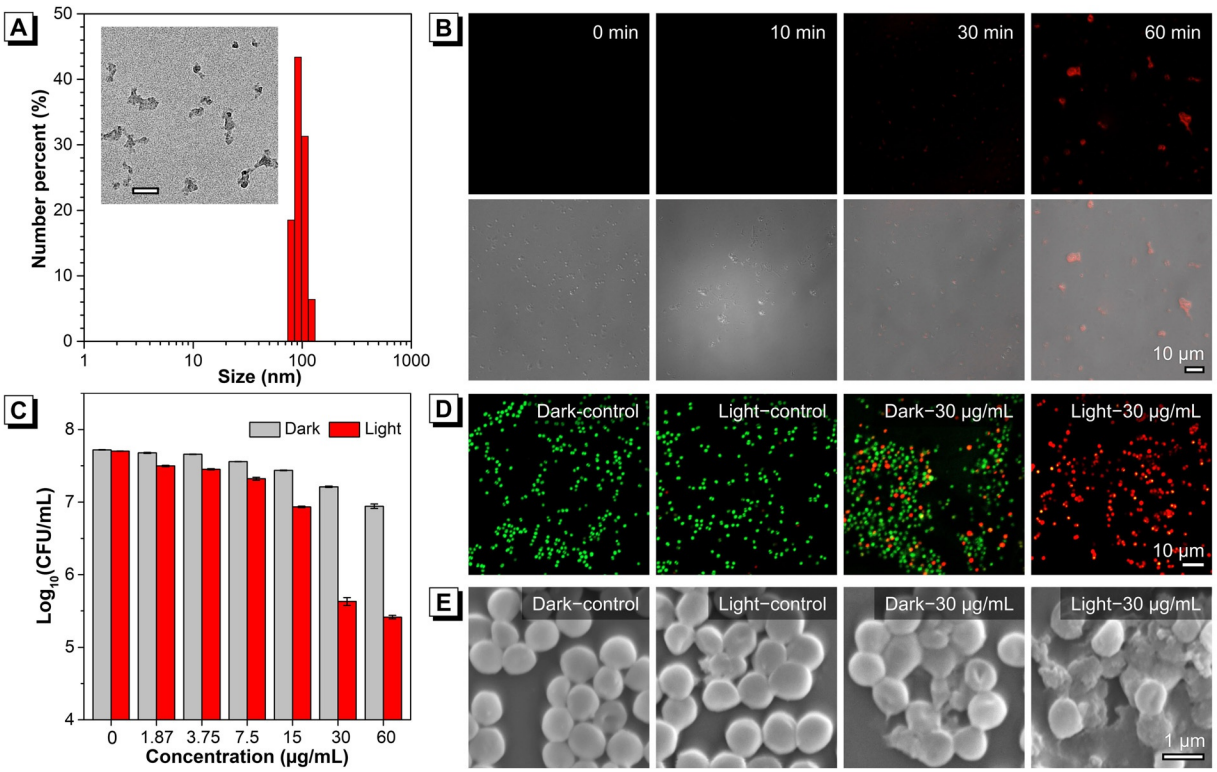

Figure 4. Antibacterial behaviors of P**1e**/**2a**. A) Size distribution of P**1e**/**2a** measured by dynamic light scattering. Inset: A TEM image of P**1e**/**2a** aggregates. Concentration: 30 μg mL^{-1}. Scale bar: 100 nm. B) CLSM images of bacteria incubated with P**1e**/**2a** for different time, where P**1e**/**2a** was shown in red. C) Statistical analyses of the bacterial viability by the logarithm number in the absence and presence of white-light irradiation. D) Live/dead staining of bacteria with different treatments, where live and dead bacteria were shown in green and red, respectively. E) SEM images of bacteria with different treatments.

MRSA by P**1e**/**2a** in the presence or absence of white-light irradiation (Figure S40 and Figure 4C). In the dark, there was a moderate concentration-dependent inhibition on the bacterial viability, which was attributed to the membrane-damaging effect of the positively charged polymers. In contrast, the viability significantly decreased by two orders of magnitude in the presence of white-light irradiation due to the additional destructive effect by the produced ROS by P**1e**/**2a**. When the concentration of P**1e**/**2a** reached 30 μg mL^{-1}, the bacterial killing efficiency was determined to be 99.2%, which indicated the outstanding photodynamic effect of P**1e**/**2a**. To visualize the antibacterial effect of P**1e**/**2a**, live/dead dual-color fluorescent staining was performed. As shown in Figure 4D, a large proportion of MRSA incubated with P**1e**/**2a** were stained with green fluorescence in the absence of light irradiation, indicating the relatively large survival rate and weak antibacterial effect. In contrast, the ratio of red fluorescence was remarkably increased in the presence of light irradiation, and no green fluorescence could be found. These results were in accordance with the aforementioned quantitative study. Furthermore, the morphology of MRSA upon different treatments was characterized by scanning electron microscopy (SEM, Figure 4E). After treated with P**1e**/**2a** in the absence of light irradiation, the smooth membrane surface of the bacteria became rough and was partially collapsed. When irradiated with white light, the bacteria were damaged with serious membrane splitting and deformation due to the photodynamic effect of P**1e**/**2a**.

Considering the high photokilling efficiency of P**1e**/**2a** toward bacteria, it is possible to explore its new application in photo-patterning of living organisms, which allows for the creation of adaptive, customizable, and dynamic bio-architectures to investigate their potential in cell migration, tissue engineering, and biochips.[36] Because light is a low-cost and noninvasive manipulation tool with high spatiotemporal resolution, we decided to fabricate living bacterial patterns by means of the photodynamic effect of P**1e**/**2a**, in which green fluorescent protein (GFP)-expressing *S. aureus* was employed to visualize the dynamic change of the resulting biopatterns. As shown in Figure 5A, the dilute bacterial solution mixed with P**1e**/**2a** was irradiated by white light through a pre-printed gridlike adhesive mask for 20 min. The ROS generated by the polymers efficiently killed the bacteria in the unmasked region, while the bacterial viability in the masked region remained unaffected. Further incubation of the whole set-up in the dark favored the rapid growth and proliferation of the GFP-expressing *S. aureus* in the masked region, leading to the formation of an array of bacterial grids that were replicated from the mask. We then monitored the dynamic change of the produced biopatterns at 12, 18, 24, and 36-h post-incubation (Figure 5B). For the group incubated with P**1e**/**2a** and irradiated with white light, a clear gridlike pattern could be identified, which became denser in the

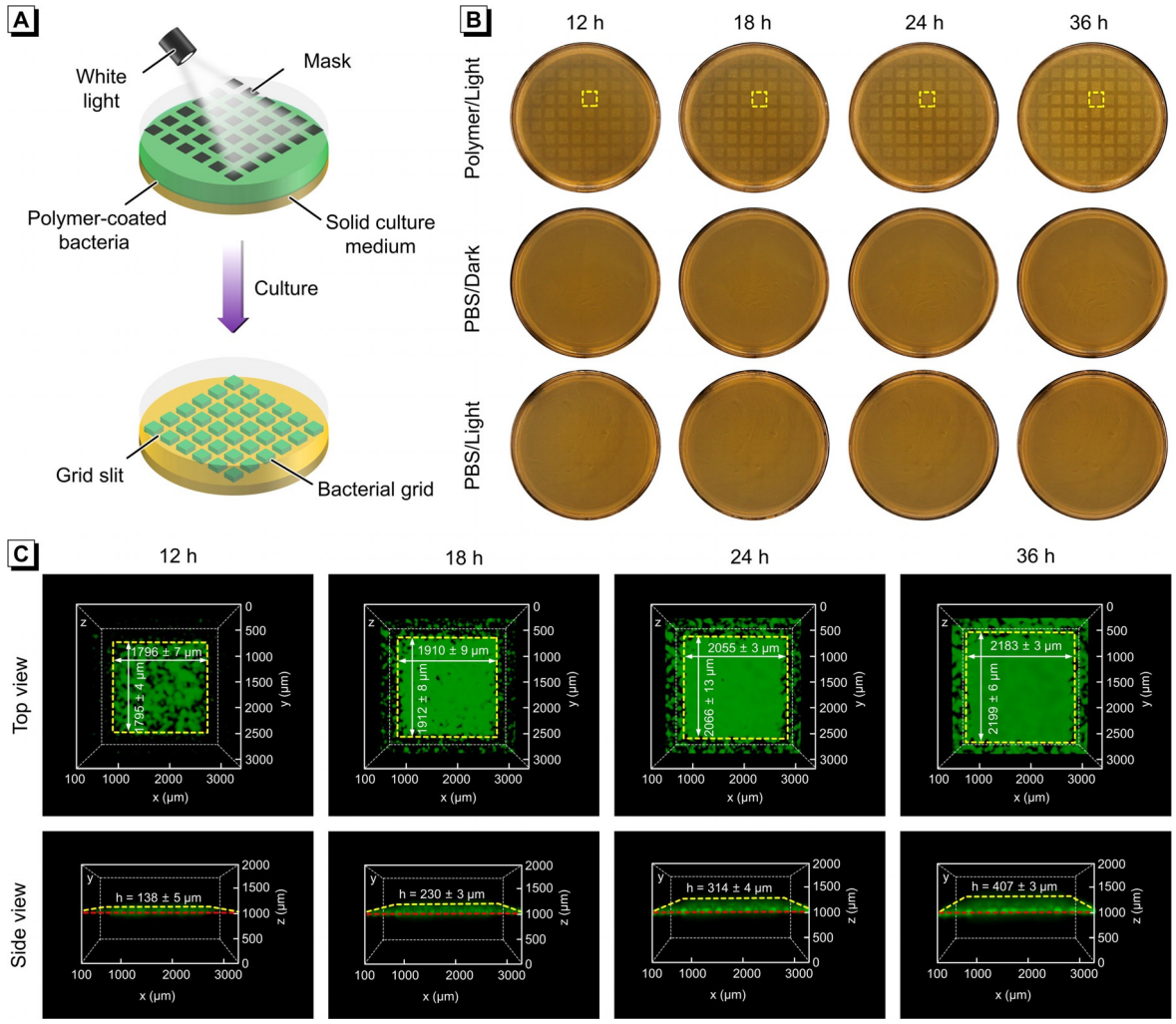

Figure 5. Photodynamic patterning of bacteria with P**1e**/**2a**. A) Illustration showing the bacterial patterning with a white light source and a pre-printed adhesive mask. B) Photographs of the bacterial pattern taken under a sun lamp at 12, 18, 24, and 36-h post white-light irradiation. "Polymer/Light" and "PBS/Light" represent the groups that were incubated with P**1e**/**2a** and PBS, respectively, followed by white-light irradiation, while "PBS/Dark" indicates the group that was incubated with PBS only. The yellow dashed rectangles outline the region of interest presented in the CLSM images. C) Three-dimensional CLSM images of a bacterial grid viewed from top and side views. The yellow dashed lines outline the border of the bacterial grid, while the red line indicates the bottom plane of the bacterial grid. The bacteria were shown in green.

masked region (i.e. grid) and coarser in the unmasked region (i.e. slit) over time. In contrast, no evident gridlike patterns were created for the control groups without the addition of P**1e**/**2a**. Such results were also confirmed by the corresponding fluorescence images taken under a 365-nm UV lamp (Figure S41). To gain more insight into the details of bacterial growth, we employed confocal laser scanning microscopy (CLSM) to characterize the three-dimensional (3D) structure of the living bacterial patterns (Figure 5C). At 12-h post-incubation, a representative grid was sparse in shape, which was characterized by a typical size of 1796 ± 7 µm × 1795 ± 4 µm with a height of 138 ± 5 µm. Upon extending the incubation time, the grid gradually expanded, and the corresponding dimensional parameters changed to 2183 ± 3 µm × 2199 ± 6 µm × 407 ± 3 µm at 36-h post incubation. Meanwhile, the fluorescence in the slit started to emerge and eventually merged with the grid, and the spacing distance between adjacent grids was narrowed from 960 ± 2 µm at 12-h post incubation to 551 ± 8 µm at 36-h post incubation (Figure S42). As photodynamic biopatterning provided a simple and cost-effective way to fabricate 3D living biopatterns, the present results thus demonstrated the potential of these hyperbranched polyelectrolytes in photo-manipulating the biological behaviors of living organisms.

Conclusion

We developed an efficient multicomponent polymerization to in situ generate functional heteroaromatic hyperbranched polyelectrolytes using readily accessible internal diynes and low-cost, commercially available arylnitriles, $NaSbF_6$, and H_2O/AcOH in a one-pot manner. Compared with conventional synthetic approaches, the present strategy involved neither unstable and expensive monomers nor strictly controlled conditions. The polymerization could

proceed efficiently with a broad spectrum of monomers, affording functional polymers in excellent yields (up to 99%) and extraordinary high molecular weights (M_w up to 1.011×10^6). Notably, all the polymers showed low $Đ$ values and high solubility in common organic solvents, regardless of their molecular weights and fused aromatic units. The positively charged heteroaromatic rings were highly electron-deficient, which facilitated the formation of D-A structures and concurrently endowed the polymers with tunable emission. The compact hyperbranched architecture of the polymers restricted their intramolecular motions to suppress the non-radiative decay to result in high fluorescence quantum yields (up to 14.3%) in the solid state, which enabled the polymers to fabricate highly ordered fluorescence photopatterns at different scales. Upon white-light irradiation, these polymers could produce considerate ROS for the efficient inactivation of bacteria. Furthermore, we, for the first time, demonstrated the possibility of the hyperbranched polyelectrolytes for the creation of customizable living bacterial patterns via PDT. The efficient multicomponent polymerization introduced here provided a facile strategy for the synthesis of hyperbranched polyelectrolytes to enrich their family members. The unique properties and functionalities of the resulting polymers offered great opportunities for a multitude of follow-up studies, such as photoelectronic materials, disease theranostics, biochips, and tissue engineering.

Acknowledgements

This work was financially supported by the National Natural Science Foundation of China (21788102 and 52003123), the Research Grants Council of Hong Kong (16305320, 16304819, 16305618, C6009-17G, and C6014-20W), the Innovation and Technology Commission (ITC-CNERC14SC01 and ITC.PD/17-9), the National Key Research and Development program of China (2018YFE0190200), the Science and Technology Plan of Shenzhen (JCYJ20170818113602462, JCYJ20180306174910791, JCYJ20170818113530705, and JCYJ20180306180231853), the National Science Foundation of Guangdong Province (2019B12120J002), the Hong Kong PhD Fellowship Scheme (PF16-02667), and the startup funds from Nankai University (to C.Z.).

Conflict of interest

The authors declare no conflict of interest.

Keywords: bacterial killing · biopatterning · multicomponent polymerization · photodynamic therapy · polyelectrolytes

[1] a) R. M. Fuoss, *Science* **1948**, *108*, 545–550; b) L. Jacques, *Science* **1979**, *206*, 528–533; c) B. Larsen, *Nature* **1975**, *258*, 344–345.

[2] L. Chen, M.-D. Ge, Y.-J. Zhu, Y. Song, P. C. K. Cheung, B.-B. Zhang, L.-M. Liu, *Carbohydr. Polym.* **2019**, *223*, 115076.

[3] S. R. Beeren, O. Hindsgaul, *Angew. Chem. Int. Ed.* **2013**, *52*, 11265–11268; *Angew. Chem.* **2013**, *125*, 11475–11478.

[4] B. Deng, M. A. Sullivan, J. Li, X. Tan, C. Zhu, B. L. Schulz, R. G. Gilbert, *Glycoconjugate J.* **2015**, *32*, 113–118.

[5] L. Yu, G. E. Yakubov, W. Zeng, X. Xing, J. Stenson, V. Bulone, J. R. Stokes, *Carbohydr. Polym.* **2017**, *165*, 132–141.

[6] P.-e. Jansson, L. Kenne, B. Lindberg, *Carbohydr. Res.* **1975**, *45*, 275–282.

[7] L. Chen, W. N. Cheng, B. B. Zhang, P. C. K. Cheung, *RSC Adv.* **2016**, *6*, 112260–112268.

[8] a) K. L. Wooley, C. J. Hawker, J. M. J. Frechet, *J. Am. Chem. Soc.* **1991**, *113*, 4252–4261; b) D. Wang, T. Zhao, X. Zhu, D. Yan, W. Wang, *Chem. Soc. Rev.* **2015**, *44*, 4023–4071; c) A. M. Nyström, K. L. Wooley, *Acc. Chem. Res.* **2011**, *44*, 969–978; d) X. Liu, T. Han, J. W. Y. Lam, B. Z. Tang, *Macromol. Rapid Commun.* **2021**, *42*, 2000386.

[9] a) J. K. Gooden, M. L. Gross, A. Mueller, A. D. Stefanescu, K. L. Wooley, *J. Am. Chem. Soc.* **1998**, *120*, 10180–10186; b) H.-T. Chang, J. M. J. Fréchet, *J. Am. Chem. Soc.* **1999**, *121*, 2313–2314; c) C. Gao, D. Yan, *Prog. Polym. Sci.* **2004**, *29*, 183–275.

[10] Y. Zheng, S. Li, Z. Weng, C. Gao, *Chem. Soc. Rev.* **2015**, *44*, 4091–4130.

[11] a) T. Emrick, H.-T. Chang, J. M. J. Fréchet, *Macromolecules* **1999**, *32*, 6380–6382; b) K.-Y. Pu, K. Li, J. Shi, B. Liu, *Chem. Mater.* **2009**, *21*, 3816–3822; c) G. Feng, J. Liang, B. Liu, *Macromol. Rapid Commun.* **2013**, *34*, 705–715; d) K.-Y. Pu, J. Shi, L. Cai, K. Li, B. Liu, *Biomacromolecules* **2011**, *12*, 2966–2974.

[12] B. Song, R. Zhang, R. Hu, X. Chen, D. Liu, J. Guo, X. Xu, A. Qin, B. Z. Tang, *Adv. Sci.* **2020**, *7*, 2000465.

[13] C. J. Galvin, J. Genzer, *Prog. Polym. Sci.* **2012**, *37*, 871–906.

[14] C. Zhu, L. Liu, Q. Yang, F. Lv, S. Wang, *Chem. Rev.* **2012**, *112*, 4687–4735.

[15] a) C. E. Arcadia, E. Kennedy, J. Geiser, A. Dombroski, K. Oakley, S.-L. Chen, L. Sprague, M. Ozmen, J. Sello, P. M. Weber, S. Reda, C. Rose, E. Kim, B. M. Rubenstein, J. K. Rosenstein, *Nat. Commun.* **2020**, *11*, 691; b) L. A. Wessjohann, E. Ruijter, D. Garcia-Rivera, W. Brandt, *Mol. Diversity* **2005**, *9*, 171–186.

[16] a) A. B. Cook, S. Perrier, *Adv. Funct. Mater.* **2020**, *30*, 1901001; b) D. Wang, Y. Jin, X. Zhu, D. Yan, *Prog. Polym. Sci.* **2017**, *64*, 114–153.

[17] a) Y. Zhou, W. Huang, J. Liu, X. Zhu, D. Yan, *Adv. Mater.* **2010**, *22*, 4567–4590; b) W. Xu, P. A. Ledin, V. V. Shevchenko, V. V. Tsukruk, *ACS Appl. Mater. Interfaces* **2015**, *7*, 12570–12596.

[18] J. Wang, X. Gu, P. Zhang, X. Huang, X. Zheng, M. Chen, H. Feng, R. T. K. Kwok, J. W. Y. Lam, B. Z. Tang, *J. Am. Chem. Soc.* **2017**, *139*, 16974–16979.

[19] a) Y.-N. Jing, S.-S. Li, M. Su, H. Bao, W.-M. Wan, *J. Am. Chem. Soc.* **2019**, *141*, 16839–16848; b) F. Hu, S. Xu, B. Liu, *Adv. Mater.* **2018**, *30*, 1801350.

[20] a) Y. Tu, Z. Zhao, J. W. Y. Lam, B. Z. Tang, *Matter* **2021**, *4*, 338–349; b) S. Tao, S. Zhu, T. Feng, C. Zheng, B. Yang, *Angew. Chem. Int. Ed.* **2020**, *59*, 9826–9840; *Angew. Chem.* **2020**, *132*, 9910–9924.

[21] a) C. Zhu, R. T. K. Kwok, J. W. Y. Lam, B. Z. Tang, *ACS Appl. Biol. Mater.* **2018**, *1*, 1768–1786; b) X. Liu, M. Li, T. Han, B. Cao, Z. Qiu, Y. Li, Q. Li, Y. Hu, Z. Liu, J. W. Y. Lam, X. Hu, B. Z. Tang, *J. Am. Chem. Soc.* **2019**, *141*, 11259–11268; c) S. Liu, H. Zhang, Y. Li, J. Liu, L. Du, M. Chen, R. T. K. Kwok, J. W. Y. Lam, D. L. Phillips, B. Z. Tang, *Angew. Chem. Int. Ed.* **2018**, *57*, 15189–15193; *Angew. Chem.* **2018**, *130*, 15409–15413; d) J. Li, K. Pu, *Acc. Chem. Res.* **2020**, *53*, 752–762.

[22] a) R. Qi, H. Zhao, X. Zhou, J. Liu, N. Dai, Y. Zeng, E. Zhang, F. Lv, Y. Huang, L. Liu, Y. Wang, S. Wang, *Angew. Chem. Int. Ed.* **2021**, *60*, 5759–5765; *Angew. Chem.* **2021**, *133*, 5823–5829; b) X. Cai, B. Liu, *Angew. Chem. Int. Ed.* **2020**, *59*, 9868–9886; *Angew. Chem.* **2020**, *132*, 9952–9970.

[23] a) S. He, Y. Jiang, J. Li, K. Pu, *Angew. Chem. Int. Ed.* **2020**, *59*, 10633 – 10638; *Angew. Chem.* **2020**, *132*, 10720 – 10725; b) J. Li, D. Cui, Y. Jiang, J. Huang, P. Cheng, K. Pu, *Adv. Mater.* **2019**, *31*, 1905091; c) X. Liu, X. Liang, Y. Hu, L. Han, Q. Qu, D. Liu, J. Guo, Z. Zeng, H. Bai, R. T. K. Kwok, A. Qin, J. W. Y. Lam, B. Z. Tang, *JACS Au* **2021**, *1*, 344 – 353; d) W. Du, X. Liu, L. Liu, J. W. Y. Lam, B. Z. Tang, *ACS Appl. Polym. Mater.* **2021**, *3*, 2290 – 2309; e) K. Xue, C. Yang, C. Wang, Y. Liu, J. Liu, L. Shi, C. Zhu, *CCS Chem.* **2021**, *3*, 531 – 544.

[24] J. Yin, F. Zhou, L. Zhu, M. Yang, Y. Lan, J. You, *Chem. Sci.* **2018**, *9*, 5488 – 5493.

[25] T. Han, Z. Yao, Z. Qiu, Z. Zhao, K. Wu, J. Wang, A. W. Poon, J. W. Y. Lam, B. Z. Tang, *Nat. Commun.* **2019**, *10*, 5483.

[26] a) J. Liu, Y. Zhong, J. W. Y. Lam, P. Lu, Y. Hong, Y. Yu, Y. Yue, M. Faisal, H. H. Y. Sung, I. D. Williams, K. S. Wong, B. Z. Tang, *Macromolecules* **2010**, *43*, 4921 – 4936; b) C. K. W. Jim, A. Qin, J. W. Y. Lam, M. Häussler, J. Liu, M. M. F. Yuen, J. K. Kim, K. M. Ng, B. Z. Tang, *Macromolecules* **2009**, *42*, 4099 – 4109.

[27] F. Wurm, H. Frey, in *Polymer Science: A Comprehensive Reference* (Eds.: K. Matyjaszewski, M. Möller), Elsevier, Amsterdam, **2012**, pp. 177 – 198.

[28] D. Chen, W. Li, L. Gan, Z. Wang, M. Li, S.-J. Su, *Mater. Sci. Eng. R* **2020**, *142*, 100581.

[29] a) C. Lü, B. Yang, *J. Mater. Chem.* **2009**, *19*, 2884 – 2901; b) G. Iasilli, R. Francischello, P. Lova, S. Silvano, A. Surace, G. Pesce, M. Alloisio, M. Patrini, M. Shimizu, D. Comoretto, A. Pucci, *Mater. Chem. Front.* **2019**, *3*, 429 – 436; c) Y. Cheng, C. Lu, B. Yang, *Recent Pat. Mater. Sci.* **2011**, *4*, 15 – 27.

[30] T. Higashihara, M. Ueda, *Macromolecules* **2015**, *48*, 1915 – 1929.

[31] J. E. Mark, *Physical Properties of Polymers Handbook*, *Vol. 1076*, Springer, Berlin, **2007**.

[32] a) Z. Nie, E. Kumacheva, *Nat. Mater.* **2008**, *7*, 277 – 290; b) G. Liu, S. H. Petrosko, Z. Zheng, C. A. Mirkin, *Chem. Rev.* **2020**, *120*, 6009 – 6047.

[33] J. Ni, Y. Wang, H. Zhang, J. Z. Sun, B. Z. Tang, *Molecules* **2021**, *26*, 268.

[34] a) H. Yuan, B. Wang, F. Lv, L. Liu, S. Wang, *Adv. Mater.* **2014**, *26*, 6978 – 6982; b) C. Schweitzer, R. Schmidt, *Chem. Rev.* **2003**, *103*, 1685 – 1758; c) C. Zhu, Q. Yang, L. Liu, F. Lv, S. Li, G. Yang, S. Wang, *Adv. Mater.* **2011**, *23*, 4805 – 4810.

[35] a) C. Wang, X. Zhao, H. Jiang, J. Wang, W. Zhong, K. Xue, C. Zhu, *Nanoscale* **2021**, *13*, 1195 – 1205; b) D. Wang, H. Su, R. T. K. Kwok, X. Hu, H. Zou, Q. Luo, M. M. S. Lee, W. Xu, J. W. Y. Lam, B. Z. Tang, *Chem. Sci.* **2018**, *9*, 3685 – 3693.

[36] a) A. Y. Chen, Z. Deng, A. N. Billings, U. O. S. Seker, M. Y. Lu, R. J. Citorik, B. Zakeri, T. K. Lu, *Nat. Mater.* **2014**, *13*, 515 – 523; b) S. Shen, Y. Huang, A. Yuan, F. Lv, L. Liu, S. Wang, *CCS Chem.* **2021**, *3*, 129 – 135.

Manuscript received: April 6, 2021
Revised manuscript received: May 10, 2021
Accepted manuscript online: May 14, 2021
Version of record online: June 17, 2021

